

Published in final edited form as:

Chem Biol. 2012 December 21; 19(12): 1556–1567. doi:10.1016/j.chembiol.2012.09.018.

Structure-guided Discovery of Phenyl diketo-acids as Potent Inhibitors of *M. tuberculosis* Malate Synthase

Inna V. Krieger¹, Joel S. Freundlich^{1,#}, Vijay B. Gawandi¹, Justin P. Roberts¹, Vidyadhar B. Gawandi¹, Qingan Sun¹, Joshua L. Owen¹, Maria T. Fraile², Sofia I. Huss², Jose-Luis Lavandera^{2,‡}, Thomas R. Ioerger¹, and James C. Sacchettini^{1,*}

¹Department of Biochemistry and Biophysics, Texas A&M University, College Station, Texas 77845, USA

²Tres Cantos Medicines Development Campus, Diseases of the Developing World, GlaxoSmithKline, Madrid 28760, Spain

Summary

The glyoxylate shunt plays an important role in fatty-acid metabolism, and has been shown to be critical to survival of several pathogens involved in chronic infections. For *Mycobacterium tuberculosis* (*Mtb*), a strain with a defective glyoxylate shunt was previously shown to be unable to establish infection in a mouse model. We report the development of novel phenyl-diketo acid (PDKA) inhibitors of malate synthase (GlcB), one of two glyoxylate shunt enzymes, using structure-based methods. PDKA inhibitors were active against *Mtb* grown on acetate, and over-expression of GlcB ameliorated this inhibition. Crystal structures of complexes of GlcB with PDKA inhibitors were used to guide optimization of potency. A selected PDKA compound demonstrated efficacy in a mouse model of tuberculosis. The discovery of these PDKA derivatives provides chemical validation of GlcB as an attractive target for tuberculosis therapeutics.

Introduction

Despite the availability of good first and second line therapeutics to treat tuberculosis (TB), drug resistance, latency, and persistence render TB a continuing threat to public health and pose an urgent need for the development of novel drugs (World Health Organization, 2011).

The glyoxylate shunt, which plays a central role in fatty-acid metabolism, has long been considered a potential vulnerability of *Mtb* during infection that could be exploited for developing antitubercular therapeutics (McKinney et al., 2000). The glyoxylate shunt is an anaplerotic bypass of the traditional tricarboxylic acid cycle that allows for incorporation of carbon from acetyl-CoA produced by fatty-acid metabolism. This pathway is utilized in plants, fungi, and prokaryotes, but is absent in mammals. *Mtb* has been shown to undergo significant metabolic alterations during the course of infection, among them a shift from a

© 2012 Elsevier Ltd. All rights reserved.

*sacchett@tamu.edu.

#present address: Departments of Pharmacology & Physiology and Medicine, Center for Emerging and Reemerging Pathogens, UMDNJ – New Jersey Medical School, 185 South Orange Avenue Newark, NJ 07103, USA.

‡present address: Institute for Applied Molecular Medicine (IMMA), School of Medicine, Universidad CEU San Pablo, Campus Monteprincipe. Boadilla del Monte – 28668 Madrid, Spain.

Publisher's Disclaimer: This is a PDF file of an unedited manuscript that has been accepted for publication. As a service to our customers we are providing this early version of the manuscript. The manuscript will undergo copyediting, typesetting, and review of the resulting proof before it is published in its final citable form. Please note that during the production process errors may be discovered which could affect the content, and all legal disclaimers that apply to the journal pertain.

reliance on carbohydrates to fatty acids as a principal source of carbon (Bloch and Segal, 1956). The increased reliance on fatty acid β -oxidation and gluconeogenesis in concert with a shift away from glycolysis during infection is supported by analysis of transcriptional profiles (Schnappinger et al., 2003), (Talaat et al., 2004).

The glyoxylate shunt as well as gluconeogenesis have been shown to play a crucial role in *Mtb* virulence, as both isocitrate lyase and phosphoenolpyruvate carboxykinase, the first committed steps of each pathway, are required for infection in activated macrophages and in animal models (McKinney et al., 2000; Marrero et al., 2010).

The glyoxylate shunt consists of two enzymes: isocitrate lyase (ICL) which hydrolyzes isocitrate into glyoxylate and succinate, and malate synthase (GlcB), which converts glyoxylate into malate using one molecule of acetyl-CoA. The shunt bypasses two CO₂-generating steps of the TCA cycle, allowing incorporation of carbon (via acetyl-CoA) and serves to replenish oxaloacetate under carbon-limiting conditions (Kornberg and Krebs, 1957). *Icl1* is one of the most highly up-regulated genes in *Mtb* under conditions that mimic infection (Timm et al., 2003). Further studies demonstrated the essentiality of the glyoxylate shunt for a persistent or chronic infection by showing that *Mtb* lacking *icl1* was unable to persist, and a knockout of both isoforms of *icl* could not establish an infection in mice and was rapidly cleared (McKinney et al., 2000; Muñoz-Elías and McKinney, 2005). A critical role of the glyoxylate shunt for virulence has been reported for other intracellular and fungal pathogens (Lorenz and Fink, 2001) (Dunn et al., 2009).

Targeting ICL has been a challenge, largely due to its highly polar and small active site that becomes even more constricted during catalysis (Sharma et al., 2000). To date, the most-used *in vitro* inhibitor of ICL is the succinate analog, 3-nitropropionate which has an IC₅₀ of 3 μ M (Muñoz-Elías and McKinney, 2005). In contrast to ICL, GlcB has a much more “druggable” and large active site, consisting of a 20 Å by 7 Å cavity, which normally accommodates the pantothenate tail of the acetyl-CoA. The catalytic Mg²⁺ is located at the bottom of the cavity (Smith et al., 2003; Anstrom and Remington, 2006). X-ray crystal structures of GlcB bound with substrate glyoxylate or products CoA-SH and malate (Smith et al., 2003) show that the protein conformation is nearly identical regardless of the ligand (r.m.s.d. < 0.5 Å), suggesting that catalysis occurs without significant structural rearrangements. In this paper, we report our structure-based discovery of small molecule inhibitors of *Mtb* GlcB, and pharmacological validation of GlcB as a drug target. One of the identified GlcB inhibitors with a reasonable potency and favorable toxicity, pharmacokinetic (PK) and pharmacodynamic (PD) profiles, has demonstrated efficacy in a mouse model of TB, and could serve as the basis for a novel class of antituberculars.

Results

Discovery of PDKA, and Crystal Structure of GlcB-inhibitor Complex

A focused library of thirty-five small molecules with a glyoxylate-like substructure were assayed against GlcB and ICL at a single concentration point of 40 μ g/ml; of these, nineteen showed activity against GlcB. All of the GlcB-actives were phenyl-diketo acids, exemplified by (*Z*)-2-hydroxy-4-oxo-4-phenylbut-2-enoic acid (PDKA) (Figure 1A). The parent PDKA exhibited an IC₅₀ of 2.0 μ M against GlcB, and was inactive against ICL. Based on these initial findings, approximately one hundred PDKA analogs were synthesized using readily available starting materials and straightforward chemical synthesis (Summa et al., 2004), (Zeng et al., 2008), (Pais et al., 2002), (Tumey et al., 2004), (Adams, 2008). A series of compounds was selected that demonstrated a good balance of enzyme inhibition and whole-cell activity. Aryl diketo acids have also been identified in drug-discovery projects for other

Mg²⁺-dependent enzymes, including HIV-1 integrase and HCV-polymerase, where the keto acid moiety was found to coordinate the catalytic divalent metal cation (Egbertson, 2007).

The enzyme inhibition activities of these compounds had IC₅₀s against GlcB ranging from 20 nM to >100 μM. However, the minimal inhibitory concentrations (MICs) against cultured mycobacteria were in certain cases in disagreement with the enzyme inhibition level, and had poor reproducibility. We also observed a time-dependent decrease of activity in solutions of inhibitors at room temperature, even during short periods of time. Using UV/Vis spectroscopy and HPLC analysis to assess the stability of our compounds, we found that the parent PDKA was stable in distilled, deionized water and organic solvents (DMSO, MeOH), but unstable (t_{1/2} ≈ 3 days) in cell growth media or any of several buffer solutions tested. The results from our HPLC-MS analysis were consistent with *retro*-Claisen decomposition, with acetophenone as a product. Based on previous findings (Egbertson, 2007), we reasoned that the very high degree of conjugation encompassing the PDKA molecule was the driver of the *retro*-Claisen decomposition. To avoid this decomposition, we hypothesized that the addition of a group to the *ortho*-position of the PDKA phenyl ring would twist the ring out-of-plane, reducing the degree of conjugation. The structure of the GlcB-PDKA complex showed a 37 degree twist of the phenyl ring of PDKA out-of-plane with the conjugated di-keto moiety. Therefore, we predicted that the twist due to substitution should not significantly impact binding of *ortho*-substituted PDKAs to the enzyme. Substitution at the *ortho*-position afforded an approximately ten-fold increase in compound stability to greater than 30 days half-life, and actually improved the IC₅₀ (Table 1). Identical substitutions at the *meta*- and *para*-positions had no effect on stability. The extent of conjugation of the *ortho*-substituted phenyl diketo acids in solution was indeed reduced, as evidenced by the blue shift of their respective UV absorbance peaks (λ_{max} values), when compared to PDKA and *meta*- and *para*-substituted compounds (Table 1). Moreover, the magnitude of this spectral shift correlates well with stability.

All other attempts to stabilize this chemical framework (removing either of the two keto groups, replacing the carbon between them with a nitrogen, or introducing a methyl group to the beta carbon of the diketo acid) resulted in compounds that were inactive against GlcB (data not shown). We evaluated replacement of the PDKA carboxylic acid by proven Mg²⁺ chelators (catechol, diazole, sulfone, pyridazinone, hydroxylamine), and other bioisosteres such as tetrazole, but all of these failed to afford GlcB inhibitors with promising enzyme activity (IC₅₀ > 100 μM).

We noticed that in the crystals of the glyoxylate-bound *Mtb* GlcB, Cys619 was often oxidized to cysteine-sulfenic acid, similar to *E. coli* malate synthase (Anstrom et al., 2003), resulting in a constriction at the entrance to the active site channel. The sulfenic acid is likely to be an artifact resulting from exposure to air during purification, and is not relevant to the metabolic function of GlcB (Quartararo and Blanchard et al., 2011), which should remain reduced in the reducing environment of the cell. We therefore constructed a Cys619Ala *Mtb* GlcB mutant, which exhibited ~80% of the reaction velocity of the wild-type (kinetic curve shown in Figure S1), and a ten-fold increase in acetyl-CoA K_M (from 5 to 50 μM). Examination of the crystal structure of GlcB bound to CoA (1N8W; Smith et al., 2003) shows that the Sγ of Cys619 makes a hydrogen bond with a nitrogen in the pantothenate arm of CoA, which could explain why the C619A mutant enzyme binds the co-factor with less affinity, potentially causing the slight reduction in reaction velocity. A similar Cys619Ser *Mtb* GlcB mutant has also been described as a suitable model for kinetic studies (Quartararo and Blanchard, 2011). However, with the Cys619Ala mutant, we did not observe the lag in activity reported for the Cys619Ser mutant, and elevating Mg²⁺ concentrations did not influence the activity (Figure S1). Since the IC₅₀ values of inhibitors measured for the mutated and wild-type enzymes were well-correlated (see Table S1,

compare to Table 1), the C619A mutant protein was used in all subsequent crystallographic studies and enzyme assays. Cys619 is located ~5 Å away from the ligand (as shown in Figure S2), and thus does not participate significantly in binding of these inhibitors.

The crystal structure of GlcB (C619A) complexed with PDKA was determined at 1.9 Å resolution (data collection and refinement statistics are presented in Table 2). No significant conformational changes in the protein were observed upon PDKA binding compared to structures with glyoxylate or malate and CoA bound. The backbone RMSD of the superposition between the GlcB:malate complex and the GlcB:PDKA complex is 0.32 Å over 700 C α atoms, and among 15 active-site residues, the all-atom RMSD is 0.21 Å, excluding Met631, which adopts a different conformer to accommodate the phenyl ring. The diketo acid group of the PDKA coordinates the Mg²⁺ ion in an edge-on fashion, very similar to glyoxylate (Smith et al., 2003), filling two of the six octahedral coordination sites with one of the carboxylate oxygens and the adjacent ketone oxygen (2.1 Å and 2.2 Å contact distances). Other active site interactions are illustrated in Figure 1B. Carboxylate oxygens of the inhibitor hydrogen-bonded with the backbone nitrogens of Asp462 and Leu461 (d_{O-N} = 3.0 and 3.0 Å, respectively). Both ketone oxygens also form hydrogen bonds (d_{O-N} = 2.9 and 2.9 Å) with the Arg339 side-chain, exhibiting similar contacts as the substrate/product. The catalytic Asp633 (Clark et al., 1988) side-chain oxygen was within hydrogen bonding distance (3.2 Å) to the phenyl ketone oxygen of PDKA. As noted above, the aryl ring of the PDKAs was twisted 37 degrees out of coplanarity with the ketone, and occupied the approximate middle of the active site channel, overlapping the region where the thiol group of CoA normally binds. The aromatic ring forms multiple van der Waals interactions with the C γ of catalytic Asp633, and the side-chains of Met515, Trp541, and Met631. The carboxylate of the side-chain of Asp633, expected to be deprotonated in view of its catalytic function (Clark et al., 1988), is positioned over the face of the PDKA ring, slightly shifted toward the diketo acid side, with distances from O δ 1 to PDKA atoms C1 and C6 of 4.1 and 3.4 Å, respectively, and from O δ 2 to C1 and C2 – of 3.3 and 4.0 Å.

The close contact between Asp633 side chain and the aryl ring of the inhibitor is unusual, and resembles anion- π interactions that have recently been reported in small molecules and proteins (Berryman et al., 2007), (Schottel et al., 2008). In most interactions between anions and aromatic groups in biomolecular systems, the anion contacts the aromatic ring on the edge (co-planar) with distances around ~4.5 Å, whereas the contacts of carboxylates over the center of the ring were generally >5.0 Å (Jackson et al., 2007), (Philip et al., 2011). However, face-on anion- π contacts have been observed in inorganic systems, and are enhanced by electron-withdrawing substituents, resulting in lower contact distances and higher binding affinities. This is supported by semi-empirical quantum mechanics calculations for representative model systems that suggests there is a significant energy well for face-on contacts at 3-4 Å (Berryman et al., 2007), (Schottel et al., 2008). All crystal structures of GlcB-inhibitor complexes with PDKA analogs we have solved to date exhibit a close contact between the carboxylate of Asp633 and the face of the aromatic ring of the inhibitor. Among the five structures reported in this paper, the mean distance between the closest arene carbon and either of the Asp633 oxygens is 3.1 Å, with a mean contact angle of 55 degrees relative to the ring plane, consistent with a face-on interaction. A superposition of the ring plane of the Asp633-PDKA pair with the small-molecule crystal structure of tetracyanobenzene (TCB)-NaI complex reported by Berryman et al. (Berryman et al., 2007) (Figure 2) shows a very similar configuration between the two systems. The anion of the TCB-NaI complex (iodine) superimposes on the carboxylate of Asp633 in the GlcB-PDKA structures, and is located over the periphery of the ring (the carbon connecting to the diketo acid moiety), rather than directly over the ring center as suggested by theoretical calculations (Schottel et al., 2008). Presumably this position provides additional localized polarization. Anion positioning over the periphery of the ring rather than over the

center has been hypothesized to indicate a partial charge transfer character to the interaction (Berryman et al., 2007). In single *ortho*-halogen substituted PDKAs (represented in Figure 2 by *o*-Br-PDKA) bound with GlcB, Asp633 is shifted away from the halogen by 1.7 Å (measured at Oδ2), reflecting the asymmetry created by the electron-withdrawing group, while with symmetric double *ortho*-halogen-substituted PDKA, the carboxylate of Asp633 is in the same position as with unsubstituted PDKA or *o*-Me-PDKA (Figure 2).

Given the extra room in the active site around the phenyl ring of the PDKA, we hypothesized that an alternative cyclic structure could be accommodated and might improve affinity. Several replacements for the phenyl ring in PDKA were prepared, including aliphatic moieties/rings, exemplified by cyclohexyl and adamantyl cores, but were found to be inactive against GlcB (data not shown), suggesting a strong requirement for an aromatic moiety. Other aromatic rings such as naphthylene and various heterocycles were evaluated, but were not immediately pursued due to a sub-optimal combination of enzyme inhibition, whole-cell activity against cultured mycobacteria, and pharmacokinetic profile (full SAR data to be published elsewhere). Naphthyl-, indole-, pyrrole-, and thiophene-based diketo acids were active against the enzyme with IC₅₀s ranging from 20 nM to 5 μM, with the first three failing at the level of whole-cell activity, and thiophenes displaying only low whole-cell activity (> 50 μM) (attributed to albumin binding) (data not shown). Furan-, quinoline-, benzodioxole-, and benzothiazole-based PDKAs exhibited low enzyme inhibition activity (IC₅₀s ranging from 30 to 100 μM), while thiazole-, pyridine- and pyrimidine-based PDKAs were inactive against the enzyme (data not shown).

Structure-Guided Optimization of PDKA Analogs with High Potency

Structural examination of the GlcB-PDKA complex suggested several opportunities to enhance affinity by making substitutions around the PDKA aromatic ring to optimize interactions within the active site (schematic view of substitution strategy is shown in Figure S3). Because of their importance for stability, we focused on optimizing the potency and whole-cell activity of *ortho*-substituted PDKAs. Crystal structures of complexes of GlcB with twenty of the synthesized PDKA analogs were determined at resolutions ranging from 1.8 to 2.2 Å (crystallographic statistics for 5 representative data sets are shown in Table 2; example of omit map density is in Figure S2) to evaluate whether binding modes agreed with our predictions, and to guide new ideas. The crystal structure of GlcB in complex with 2-Br-PDKA (**4**) showed that the Br oriented toward the Val118 side-chain (Figure 3A). Of the *ortho*-substituted analogs, inhibitor potency was improved compared to unsubstituted PDKA (2.0 μM), the most potent being those with halogens, with a preference for smaller groups: 2-F (0.24 μM) < 2-Cl (0.5 μM) < 2-Br (0.6 μM) < 2-Me (1.1 μM) (Table 1). This was presumably due to the increase of steric clashes with the Val118 side-chain (3.2 Å from Br to the closest Cγ of Val118). There is little space available to accommodate a larger group, and indeed, *o*-Et-PDKA showed an IC₅₀ of only 35 μM. Crystal structures of *ortho*-substituted PDKA complexes with GlcB indicated that all the *ortho*-substituents line up in the same direction, i.e. none are rotated to position 6 (Figure 1A), regardless of their size or nature, as exemplified by the crystal structure of GlcB in complex with the 2-Br derivative (**4**) (Figure 3). The ring of the *ortho*-substituted PDKA does not overlap exactly with the position of the parent PDKA ring (Figure 3), where for all of 2-substituted inhibitors it is moved about 0.7 Å away from Val118 to accommodate the group at the 2-position.

There was less room in the pocket off the 6-position of the aryl ring compared to the 2-position of the bound PDKA (3.9 Å compared to 4.35 Å to the closest protein atoms). This is likely the reason why the double *ortho*-substituted compound 2-Cl-6-F (**10**) (IC₅₀ = 2.7 μM) did not show a better inhibition against the enzyme than PDKA (IC₅₀ = 2.0 μM). However, we cannot rule out the possibility of an unfavorable alteration in the ring's

electron properties compared to a single *ortho* substituent affecting interaction with Asp633 (Figure 3A,B).

Position 4 (*para*- to the diketo acid) points directly at the Met631 side-chain (3.6 Å to Met631 C γ) (Figure 3A,B). Therefore accommodation of a substituent at this position requires the Met631 side-chain to assume a different conformation. And indeed, 4-Me and 4-Br PDKA analogs (**8** and **9**) showed higher IC₅₀ values than parent PDKA (5.7 and 6.0 μ M respectively), likely due to steric interference with the Met631 side-chain.

The structure of the PDKA bound to GlcB showed that position 3 of the aromatic ring was the most promising for extending the PDKA, as any extension should align with the long axis of the channel where the substrate acetyl-CoA binds (Figure 3). This offered the possibility of exploiting the pantothenate binding contacts: e.g. hydrogen bond with the back-bone N of Val119, and van der Waals interactions with the side-chains of Met631, Met515, and the back-bone of Val118-Val119. Indeed, analogs with substitutions at the *meta*-position showed the largest improvement in potency over PDKA, with the most active compounds being 3-Cl-PDKA (**6**, IC₅₀ = 0.17 μ M) and 3-Me-PDKA (**5**, IC₅₀ = 0.18 μ M). The crystal structure of GlcB in complex with the 3-Br-PDKA (IC₅₀ = 0.8 μ M) (**7**) showed the Br in the van der Waals contact, sandwiched between the side chains of Met515 and Met631, arranged on opposite sides of the channel. It is interesting to note that although sufficient space seemed to exist in the channel to accommodate longer substitutions at the *meta*-position, alkyl and (CH₂)_nAr (n = 1, 2; Ar = aryl) substitutions at that position resulted in inhibitors with poor enzyme activity (IC₅₀ > 100 μ M). This may be attributed to a sub-optimal angle at which the *meta*-substituents project off the phenyl ring, potentially resulting in steric clashes with either Met631, or with Val119 and Pro120 on the other side of the channel.

The substituent's effect on the electronic properties of the aromatic ring of PDKA appeared to be critical for inhibition activity. This is likely due to their influence on ring π -interactions with the carboxylate of catalytic Asp633. For example, 2-Cl-6-F substituted PDKA (**10**) has an IC₅₀ of 2.7 μ M, while 2,6-Me-PDKA which is of similar size and substitution positioning, but not electron-withdrawing, was inactive with an IC₅₀ > 100 μ M. Although the activity of compounds with halogens substituted at the 3-position had better enzyme activity than analogs substituted at the 2-position (e.g. 0.5 μ M IC₅₀ for 2-Cl-PDKA vs. 0.17 μ M for 3-Cl-PDKA), there was a tradeoff with stability, as 2-substituted compounds exhibited longer half-lives, and since stability was important for whole-cell assays and *in vivo* testing, we chose to pursue compounds with 2-substitutions included. Tri-substituted 2-Cl-6-F-3-Me-PDKA (**11**) did not result in an additive affinity of each position (IC₅₀ = 5.5 μ M). However, **11** proved to be a good candidate for future study, as its methyl ester derivative exhibited a good combination of essential features (reasonable potency, high bioavailability, low toxicity) to modulate mycobacterial growth in an animal model of TB infection.

Anti-mycobacterial Activity of PDKA Inhibitors

We carried out whole-cell testing of growth inhibition by PDKAs on 0.2% acetate-supplemented M9 media to model fatty acid-driven metabolism, and 0.2% dextrose-supplemented 7H9 media to model carbohydrate-oriented metabolism for comparison. Initial testing was conducted with a Biosafety Level 2 (BL2)-approved vaccine strain of *Mtb* with deletions of the *panCD* genes and the RD1 region (*mc*²-7000) (Sambandamurthy et al., 2006). Freshly synthesized inhibitors were solubilized immediately prior to MIC determination (presented in Table 1, 3). Almost all of the PDKA inhibitors (8 of 11 presented in Table 1) with reasonable potency against the enzyme inhibited growth of bacteria on acetate (with MICs from 6.25 μ M to 50 μ M), and were less potent on

carbohydrate (dextrose), with MICs usually 2-4 fold higher than on acetate, indicating that they affect the glyoxylate shunt. In the context of this paper, MICs are reported as MIC₉₉, which refers to the minimum concentration of a compound at which bacteria growth is inhibited by >99%, as assessed by absence of respiration in the rezasurin (AlamarBlue) assay. Testing on other tuberculosis strains and clinical isolates has not yet been carried out.

To improve whole-cell activity, we employed a prodrugging strategy by masking the acid via esterification as a way to enhance cellular uptake. Simple alkyl esters of whole-cell-active PDKA analogs had approximately 8-fold lower MICs compared to their corresponding PDKAs (Table 3). Of particular interest were the ester prodrugs of the *ortho*-bromo (**4**), *ortho*-methyl (**5**), and 2-chloro-6-fluoro-3-methyl (**11**) PDKAs, exhibiting MIC values in the 1 to 8 μ M range against H37Rv grown on acetate as a carbon source (Table 3). In agreement with earlier data on the *Mtb* mc²-7000 strain, PDKA esters inhibited growth of an H37Rv strain on dextrose supplemented media with a 2-4 fold higher MICs. In addition, Caco-2 uptake studies (Yazdani et al., 1998) demonstrated the enhanced permeability of esters compared to their corresponding acids (from a non-detectable level for acid **11** to a high level of 371 nm/s for the corresponding methyl-ester **12**), suggesting they could potentially be orally bioavailable and taken up through the gut. Following the decomposition of the benzyl- and methyl-esters of **11** in whole-cell lysates over time by mass spectrometry demonstrated accumulation of acid **11**, and no other product (Table S2). As expected, none of the PDKA esters themselves were directly active against GlcB in the enzyme assay, but upon hydrolysis with longer pre-incubation, each ester decomposed to yield the parent PDKA (free acid) active against the enzyme. Furthermore, PDKA esters inhibited malate synthase activity in mycobacterial cell lysates (Table S1, S2). These compounds achieved IC₅₀s in whole-cell lysates similar to the purified enzyme assay, with no loss of inhibition even after 3 hours of incubation due to potential reactivity or binding to other proteins, arguing that these compounds act on GlcB inside the cell (Table S1).

The methyl ester of **11** (**12**) was tested using the standard minimal bactericidal concentration (MBC) determination protocol (Motyl et al., 2006), and shown to be bactericidal to mc²-7000 in culture on either acetate or dextrose carbon sources. The MBC was approximately the same as the MIC when grown on acetate, and the MBC was 2-4 fold higher than the MIC on dextrose. Compound **12** was also tested in the Low-Oxygen Recovery Assay (LORA), one of the *in vitro* models of the non-replicating drug-tolerant state of *Mtb* (Cho et al., 2007), and was found active against H37Rv grown on dextrose (MIC = 52 μ M). The observed 4- to 5-fold shift of MIC in the LORA assay compared to the MABA assay (Microplate Alamar Blue Assay; Franzblau et al., 1998) (MIC = 11 μ M) is consistent with what has been observed for other antitubercular drugs with activity against non-replicating bacteria, such as rifampicin (Cho et al., 2007).

To confirm that GlcB is the intracellular target responsible for growth inhibition in *Mtb* we constructed a GlcB-overexpressing strain in *Mtb* containing on a plasmid either GlcB under a tetracycline-inducible promoter, or an unrelated *Mtb* protein (Rv3547) as a control. An 8-fold increase in the MIC (12.5 to 100 μ M) was observed after induction of GlcB expression using anhydrotetracycline on M9 media with acetate, and a 4-fold increase in the MIC (25 to 100 μ M) on 7H9-dextrose, whereas the strain with the control plasmid (Rv3547) showed no shift in MIC for compound **12**. All strains displayed the same MIC for rifampicin (with or without anhydrotetracycline) as the untransformed parental strain. The observed increase in the MIC for compound **12** in response to GlcB overexpression strongly supports on-target activity. In addition, we have tested PDKA inhibitors (**4** and **11**) at a high concentration of 100 μ M on four purified enzymes in the core metabolic pathways from *Mtb* which react with similar substrates (ICL, phosphoenolpyruvate carboxykinase, isocitrate dehydrogenase,

and pyruvate kinase) and observed no inhibition (data not shown), adding to reassurance that inhibition is specific to GlcB.

Inhibition of GlcB in a Murine Model of TB

We evaluated the pharmacologic properties of several of the most potent inhibitors and selected a representative for advancement to a mouse model of TB infection. The most important factors we considered were solubility, chemical stability, plasma protein binding, serum stability, metabolic clearance in microsomes, and pharmacokinetic profile. The ADME guidelines we used were: soluble in PBS at >20 g/ml; stability in human and murine plasma > 70% over 1 h; extent of plasma protein binding known; clearance in mouse microsomes after 30 min < 15 ml/min/kg, and Caco-2 permeability > 10×10^{-6} cm⁻¹/s. The methyl ester **12** showed the best combination of potency with *in vitro* pharmacokinetic (PK) properties among the PDKA analogs tested (Table 3), and therefore was selected for further *in vivo* PK, pharmacodynamic (PD) and toxicity studies. In mice, **12** was orally bioavailable (%F = 92) and attained sufficient blood levels (i.e., at 600 mg/kg dosing: T_{max} = 0.25 h, C_{max} = 99.5 μg/ml, and AUC_{8h} = 54.3 μg*h/ml). **12** demonstrated good stability in CD1 mouse plasma, in terms of slow hydrolysis of the ester to yield the parent PDKA derivative (t_{1/2} = 30 min, conversion from **12** to **11** in plasma). The corresponding acid, **11**, demonstrated a low rate of clearance in a mouse liver microsome assay (<0.3 ml/min*g), , and a reasonable level of mouse plasma protein binding (70%). (The eventual disposition of **11**, whether by metabolism or excretion, was not determined *in vivo*.) The achieved exposure for **12** in mice, as measured by AUC_{free}/MICH37Rv/acetate (35 @ 600 mg/kg oral dosing), compared reasonably well to clinical antituberculars such as moxifloxacin (AUC_{free}/MICH37Rv/acetate = 142 @ 100 mg/kg oral dosing), which is used in treatment of multi-drug resistant tuberculosis (MDR-TB) (Cox et al., 2011). (PK curves for **12** and its activated form **11** are shown in Figure S4.) The PK data show that the peak blood concentration achieved for compound **12** at 300, 500, and 600 mg/kg was approximately 150-200 fold higher than the MIC for H37Rv (2 μM=0.548 μg/ml), and the exposure was maintained above the MIC value for at least 6-7 hours. Assessment in C57BL/6J mice with a single-dose oral administration of **12** formulated in Solutol (30%) and PEG 400 (70%) demonstrated that a dose of 1000 mg/kg (the highest tested) was not lethal, and the maximum tolerated dose (MTD) was determined to be 600 mg/kg. No toxicity effects were observed at 400 mg/kg po twice daily.

Compound **12** was tested in a murine model of acute TB infection (Rullas et al., 2010). C57BL/6J mice were infected intratracheally with 10⁵ CFU and treated for 9 days, followed by determination of bacillary load in the lungs. Several dosing strategies from 300 to 600 mg/kg were tested to determine the best compound exposure above the MIC at or below the MTD established. Treatment with moxifloxacin (30 mg/kg) was used for comparison. At all dosing levels (once daily (uid) and twice daily (bid)), **12** exhibited a statistically significant reduction (p-values < 0.0001) in the *Mtb* bacterial load compared to the control (Table 4). In fact, at 400 mg/kg bid dosing, **12** reduced the bacterial load by over 100-fold (Δlog₁₀ CFU = 2.12), within an order of magnitude of moxifloxacin (Δlog₁₀ CFU = 3.07). This activity was achieved despite the fact that the dosage, which was limited by the MTD, provided exposure well above the MIC for only 6-8 hours at a time. Thus, inhibition of GlcB resulted in impairment of the ability to establish an acute infection in mice, similar to the results obtained with a Δ*icl1/2* strain (Muñoz-Elías and McKinney, 2005).

Discussion

Our studies have shown that malate synthase is essential for *Mtb* survival both *in vitro* and *in vivo*, and this enzyme can be targeted with phenyl-diketo acid (PDKA) inhibitors.

Structure-guided design led to the identification of highly potent inhibitors with sub-micromolar IC₅₀s. While the acids in the series displayed difficulty penetrating the cell wall, esters of these compounds acted as prodrugs that could be taken up and hydrolyzed inside cells, leading to potent growth inhibition. Over-expression of the enzyme leads to a ~4-fold increase in MIC for these compounds - evidence that GlcB is the target whose inhibition is responsible for cell death. Furthermore, we observed a correlation in structure-activity relationship, where analogs with different substituents around the PDKA core that inhibit the enzyme (or their corresponding esters) also inhibit whole-cell growth, and analogs with substituents that abrogate activity against the enzyme are also inactive (even in their ester forms) against whole-cells. This correlation of SAR would be highly unlikely if the actual target of these compounds inside the cell were an enzyme other than GlcB. Finally, the compounds are consistently 4-fold more potent in cultures grown on acetate as a carbon source compared to dextrose - conditions where cells rely on the glyoxylate shunt. Based on these observations, we conclude that inhibition of GlcB is the mechanism of action of the PDKAs *in vivo*.

The observation that inhibitors of GlcB are bactericidal for *Mtb* grown on carbon sources other than fatty acids, such as carbohydrates like dextrose, was unexpected because inactivation of ICL is tolerated when grown *in vitro* on carbohydrates (McKinney et al., 2000). Since ICL2 also has partial isocitrate lyase activity (Gould et al., 2006), a $\Delta icl1/icl2$ double mutant of *Mtb* completely lacking a functional glyoxylate shunt was constructed, and was also found to be able to grow on dextrose (Muñoz-Elías and McKinney, 2005). However, the $\Delta icl1/icl2$ double mutant grew at a suppressed rate (2-4 day lag), and this growth defect suggests that the glyoxylate shunt might be playing a metabolic role even when *Mtb* is growing on carbohydrates. Unlike *E. coli* and other well-studied bacteria, which suppress anaplerosis in the presence of a preferred carbon source like carbohydrates (Fischer and Sauer, 2001), *Mtb* catabolizes carbohydrates and fatty acids concurrently *in vitro* with no apparent repression (Carvalho et al., 2010).

Supporting the observation that GlcB is essential *in vitro*, recent high-density transposon-mutagenesis experiments (analyzed by deep sequencing) have shown that *glcB* is essential for growth on glycerol (representative of carbohydrates), as well as on cholesterol as a carbon source (Griffin et al., 2011).

One possible explanation for the requirement for GlcB could be to avoid accumulation of glyoxylate, which has been shown to be toxic in other bacteria (Nuñez et al., 2001). However, *Mtb* is able to grow on glyoxylate as a sole carbon source (our unpublished data), and there are other enzymes (i.e. glycine dehydrogenase or glyoxylate aminotransferase) that can utilize glyoxylate as a substrate (Sakuraba et al., 2008), (Wayne and Lin, 1982). In addition, we found, that when the ICL inhibitor 3-nitropropionate (3-NP) is co-administered at a low sub-MIC concentration (20 μ M) with GlcB inhibitors to *Mtb* cultures grown on 7H9-dextrose media, it causes a *decrease* in MIC (for example, from 12.5 μ M to 1.56 μ M for **12**). In theory, the presence of 3-NP should reduce glyoxylate accumulation by suppressing flux through the glyoxylate shunt, and would thus be expected to cause an increase in MIC for GlcB inhibitors. The decrease in MIC we observed suggests that the requirement for GlcB *in vitro* under carbohydrate-supplemented growth conditions might not be limited to a need for glyoxylate detoxification.

There are several alternative reasons why GlcB inhibition under carbohydrate-supplemented growth conditions might result in cell death. Functional GlcB might be required when grown on dextrose to replenish the intermediates on the reductive side of TCA cycle (succinate, malate, and oxaloacetate), which were shown to be maintained at relatively low intracellular concentrations by metabolite tracing (Carvalho et al., 2010). A recent analysis of ¹³C

metabolic flux in *Mtb* demonstrated a constant flux through the glyoxylate shunt, even with a carbohydrate (glycerol) as a carbon source, and that disruption of *ic11* resulted in a loss of viability at a slow growth rate (Beste et al., 2011). This echoes the finding of ICL1 being important to *Mtb*'s ability to adapt to nutrient-limiting conditions by regulating ATP levels required for entering a non-replicating state (Gengenbacher et al., 2010). These data point to the conclusion that the role of the glyoxylate shunt extends beyond its anaplerotic function in *Mtb*. Despite the uncertainty about its metabolic role under carbohydrate-supported growth conditions, our results make it clear that inhibition of GlcB is lethal to *Mtb* grown on multiple carbon sources, and this provides a novel route to antitubercular drug development.

Significance

Novel enzyme targets are needed to drive discovery of new drugs for combating tuberculosis. Because of its role in the glyoxylate shunt, we have investigated malate synthase (GlcB) as an attractive target and identified a series of potent inhibitors with a phenyl-diketo acid (PDKA) scaffold. A selected compound (**12**) in the PDKA series was shown to have efficacy in a mouse model of infection. While complete sterilization was not achieved, the bacterial load was reduced nearly 100-fold over the course of 9 days. Interestingly, the compound appears to be active during the acute phase of infection, which is consistent with the essential role of GlcB for growth on other carbon sources in addition to fatty acids. Thus, these compounds have the potential to have activity during both acute and chronic phases of infection. It is likely that with further optimization, a more potent compound than **12** (which was chosen for a tradeoff of PK/PD properties) would be able to achieve even higher bacterial clearance *in vivo*. Nonetheless, the statistically significant reduction of the bacterial load observed indicates that the PDKA compounds could have therapeutic potential, and provides evidence that *Mtb* GlcB could be a clinically-relevant target. These structural studies will form the foundation for development of better GlcB inhibitors to eventually be used in human clinical trials.

Experimental procedures

Protein overexpression and purification

GlcB with the Cys619 mutated to Ala was cloned into a custom vector *p6HisF-11d*, expressed in *E. coli* BL21 cells, and purified by Ni affinity and size exclusion columns as described previously (Smith et al., 2003). As the presence of the His-tag did not change the results of the enzyme assay or crystallization, most of the reported work was done using GlcB with the N-terminal His-tag intact.

DTNB-coupled enzyme assay

For the C619A GlcB mutant enzyme, a DTNB-coupled assay was used to evaluate inhibition activity. A BMG POLARstar OPTIMA plate reader was used to determine the inhibition of GlcB by continuously monitoring the formation of CoA in the forward enzymatic reaction by the increase in absorbance at 412 nm due to 5,5'-dithiobis-(2-nitrobenzoic acid) (DTNB)-CoA adduct formation, over a period of 20 minutes. The 96-well plates contained 100 μ l total reaction volume with 13 nM C619A GlcB in the reaction buffer (20 mM Tris pH 7.5 and 5 mM MgCl₂). All inhibitors (in 100% DMSO) were added such that the final reaction mixture contained 1% DMSO. Inhibitors were incubated with GlcB in the reaction buffer for 20 min at room temperature before adding 0.6 mM acetyl-CoA. The reaction was initiated by the addition of 1.2 mM glyoxylate and 0.5 mM (final concentration) DTNB. Each data point for the IC₅₀ plots was measured in triplicate. The data reported in this paper reflect the most robust enzyme assay conditions. We noticed that a longer pre-incubation time with GlcB (probed up to 3 hours), and lower Mg²⁺

concentrations in the assay buffer (1-5 mM, still in vast excess to the K_M for this metal ion as a co-factor in the reaction) led to enhanced enzyme inhibition for the PDKA family of inhibitors (relative to control reactions of the enzyme incubated for the same duration, in the same Mg^{2+} concentrations without inhibitor in each case, which corrects for the slight loss of activity of the enzyme over time due to protein instability). It appears that PDKA inhibitors are slow to reach equilibrium binding, probably because they bind through chelating Mg^{2+} in the same manner as glyoxylate (Copeland, 2005). However, incubating longer than 30 minutes at room temperature led to a decrease in enzyme velocity and reduced assay reproducibility, and was not done for routine inhibitor testing aiming at building SAR.

Pyruvate dehydrogenase (PDH)-coupled assay

For the wild-type GlcB enzyme, this assay was used because the Cys619 in the active site is sensitive to oxidation by the DTNB in the coupled reaction. Velocity was measured by monitoring the increase of fluorescence (excitation at 340 nm, emission at 480 nm) due to NADH production coupled with the release of CoA-SH. Final concentrations in the reaction mixture were: 3 nM of GlcB, 0.1 UI/ml of PDH, 50 μ M glyoxylate, 2 μ M acetyl CoA, 500 μ M NAD, 500 μ M pyruvate, 200 μ M thiamine pyrophosphate, 5 mM $MgCl_2$, 0.8 mM EDTA, 50 mM Tricine pH 7.4. EDTA was included in the assay buffer in both assays because it enhances the stability of the enzyme and does not affect the enzyme velocity, though it is over 6-fold lower than the concentration of Mg^{2+} used. The same assay was used in mycobacterial (BCG) cell lysate (1 mg/ml total protein concentration measured by Bradford assay), with cells harvested at mid-log phase and disrupted by sonication.

Inhibitor synthesis

Chemical syntheses of the PDKA compounds used in this study are described in the Supplemental Information. Chemical structures for compounds **1-12** are shown in Figure S5.

Protein crystallization, data collection, and data analysis

Purified C619A GlcB (with His₆ tag) at a concentration of 5 mg/ml in 20 mM Tris-HCl pH 7.5 buffer with 0.1 M NaCl was mixed for crystallization with an equal volume of mother liquor of 18-22% PEG 3350, 0.1 M $MgCl_2$, and 0.1 M Tris-HCl pH 8.0. Crystals were obtained by hanging drop vapor diffusion within 2-3 weeks. Inhibitors were soaked in by transferring pre-formed GlcB crystals into a drop made from mother liquor with 1-5 mM of inhibitor added from a DMSO stock solution such that the final DMSO concentration was below 1%, and incubated for 1-5 days. Prior to data collection crystals were cryo-protected by Fomblin (Sigma), and flash frozen in liquid nitrogen. Data were collected at Argonne National Lab APS synchrotron, beamlines 19- and 23-ID, at 0.98 Å. Diffraction data were indexed, integrated, and scaled in HKL2000 (Otwinowski and Minor, 1997). Data were truncated in CCP4 (1994). 1N8I (Smith et al., 2003) with only the protein atoms included in the refinement was used as the model for the initial rigid body refinement of the isomorphous P4₃2₁2 crystal in REFMAC (Murshudov et al., 2011). Then iterative runs of inspection and manual modification in COOT (Emsley et al., 2010) and refinement in PHENIX (Adams et al., 2002) with simulated annealing were done to gradually improve the model. The ligand model and dictionary files were created in ELBOW BUILDER from the PHENIX suite, and fitted into the density in COOT. Final refinement was done in BUSTER (Bricogne G, 2010). For data collection and refinement statistics see Table 2. All ligands had strong electron density in the 2Fo-Fc map covering all atoms visible (example shown in Figure S2). After refinement, the halogens in halogen-containing inhibitors displayed negative Fo-Fc peaks over them in the Fourier difference map. This might have been an artifact due to radiation damage, as refinement with data truncated to very low-redundancy

reflections showed no negative Fo-Fc density at these sites. For final model refinement, high redundancy sets were used, and individual occupancies were refined for halogen-containing ligands to eliminate disagreement in the Fo-Fc map. Ramachandran statistics are as follows (given in order most favored/additionally favored regions/outliers in percent): GlcB-PDKA - 97.11/2.02/0.87; GlcB-4 - 97.21/1.76/0.73; GlcB-1 - 97.34/2.22/0.44; GlcB-7 - 97.27/2.16/0.58; GlcB-11 - 96.85/3.01/0.14. All of the Ramachandran outliers are on the surface of the protein except Glu273, which hydrogen bonds with a water molecule coordinating the Mg²⁺. This unusual backbone conformation is well-supported by the electron density in all data sets.

Accession numbers

Crystal structures of GlcB in complex with inhibitors were deposited in the protein data bank under entry IDs 3S9I, 3S9Z, 3SAD, 3SAZ, and 3SB0.

Whole-cell testing

MIC determination was done using the MABA (Franzblau et al., 1998) assay in 96-well plates. For the *Mtb* mc²-7000 strain (Sambandamurthy et al., 2006), cells were grown in 7H9 media with OADC (Middlebrook) supplement, 0.05% Tyloxapol (Sigma) and 25 µg/ml pantothenate to an OD₆₀₀ of 1-2. Then cells were diluted into testing media to an OD₆₀₀ of 0.01 and pipetted into testing plates, 200 µl per well. The two testing media were: 7H9 media with 0.2% dextrose, 0.085% NaCl, 0.05% Tyloxapol, and 25 µg/ml pantothenate or M9 (Sigma) media with 0.25% Na acetate, 2 mM MgSO₄, 0.1 mM CaCl₂, 0.05% Tyloxapol, and 25 µg/ml pantothenate. Then each compound was added as a 1/2 serial dilution in DMSO (2% DMSO final in a well). 7H9-dextrose plates were incubated for 6 days before staining with resazurin (Sigma), M9-acetate plates were incubated for 3 weeks, and then for additional 2 days after staining at 37 °C with shaking. The lowest concentration where resazurin stayed completely unconverted was recorded as the MIC₉₉ value. MIC₉₉ refers to the minimum concentration at which growth of the experimental strain mc²-7000 is inhibited by >99%, as assessed by absence of respiration in the resazurin (AlamarBlue) assay. Rifampicin was used as a control: for mc²-7000 *Mtb* displaying an MIC₉₉ of 0.125 µM in 7H9-dextrose, and an MIC₉₉ of 0.25 µM in M9-acetate. MIC values for rifampicin varied no more than one dilution point from run to run. All MIC₉₉ values reported are overage with 1/2 dilution precision from at least three independent experiments. For H37Rv *Mtb* strain testing, an inoculum standardized to approximately 1×10⁷ cfu*ml⁻¹ was diluted 1 in 200 in testing media of 7H9, ADC, 0.025% Tween 80, 0.085% NaCl or 7H9, 0.5% albumin, 0.1% Na acetate, 0.025% Tween 80, 0.085% NaCl. Inhibitors were tested as with the mc²-7000 strain. Plates were incubated at 37 °C for six days before and 24-48 hours after staining with resazurin.

Mouse microsomal clearance and plasma protein binding

Microsomal intrinsic clearance was measured as described by (Clarke and Jeffrey, 2001). The compound (0.5 µM) was incubated with 0.5 mg/ml microsomal protein, 0.34 mg/mL NADP, 1.56 mg/ml glucose-6-phosphate, and 1.2 units/ml glucose-6-phosphate dehydrogenase, 2.6 mg/ml UDPGA, 0.5% (v/v) methanol in 50 mM potassium phosphate buffer, pH 7.4, at 37 °C. Fifty microliter aliquots of the incubation mixture were withdrawn at various time points over 30 min and added to 100 ml stop solution (80:20:1 (v/v/v) acetonitrile:ethanol:acetic acid) containing internal standard. Samples were snap frozen and stored at -80 °C until analyzed by LC/MS/MS. Prior to analysis, samples were thawed at room temperature, vortexed, then centrifuged, and the supernatant taken for analysis. No cofactor controls were included to assess non-P450 dependent clearance. Clearance was estimated for midazolam in parallel to assure integrity of the microsomal preparations and

acceptable interassay variability. The intrinsic clearance was calculated based on the method published by (Obach et al., 1997), using the first-order elimination rate constant for disappearance of the parent compound. This was calculated from the slope of the log-transformed concentration-time curve using SigmaPlot 8.0 (Systat Software Inc). Clearances were expressed in units of ml/min/g liver. The clearance was predicted based on the assumption that the drug concentration (0.5 μ M) was most likely well below the K_M . The lower limit of quantification was 0.5 ml/min/g liver and this corresponded to <15% decrease in the parent compound in 30 min. The *in vitro* plasma protein binding of the diketo acids was determined by equilibrium dialysis (3 cells/species) in fresh mouse and human plasma at 0.5 and 5 mg/ml (0.5% (v/v) DMSO final concentration). Spiked plasma samples were mixed gently and triplicate aliquots were collected to verify initial concentrations. Following assembly of dialysis RED devices (Thermo Scientific) (MW cut off limit of 8,000 to 10,000 Da), spiked plasma was placed in the donor compartment of the cell and phosphate buffered saline, pH 7.4, in the receiver compartment. Cells were incubated in a water bath at 37 °C and mixed continuously for 6 h. Triplicate aliquots (volume determined gravimetrically) from donor and receiver compartments were snap frozen and stored at -30 °C prior to analysis. Percent binding was estimated using standard equations which accounted for volume changes due to Donnan effects (Boudinot and Jusko, 1984).

Pharmacokinetic measurement

The compound was assayed as a single oral dose at 20 mg/kg, 100 mg/kg and 600 mg/kg in female C57BL/6J mice, dissolved in PEG400/Solutol 70:30. The sampling scheme post-administration was 15, 30, and 45 minutes, 1, 1.5, 2, 3, 4, and 8 hours; 4 animals per time point. Peripheral blood levels were analysed by LC/MS/MS. Data analysis was performed with WinNonlin 5.2; Non-compartmental analysis (NCA).

Efficacy in mouse model of TB

To assess the therapeutic efficacy of compound **12** against *M. tuberculosis* in an acute murine model of intratracheal infection (Rullas et al., 2010), mice were infected with 10⁵ CFU and lung homogenates were obtained 9 days after infection (n = 4-5 mice/group for all groups). Compound **12** was administered according to the schedule indicated in Table 4 (either once a day or twice a day) using PEG400/Solutol 70:30 as the vehicle. Moxifloxacin (30 mg/kg) dissolved in Captisol 20% was used as quality control of the assay, and reduced the CFU lung number by 3.07 logs with respect to untreated mice. The average log CFU in the lungs of untreated mice was 7.13.

Supplementary Material

Refer to Web version on PubMed Central for supplementary material.

Acknowledgments

The authors would like to thank Dr. Franzblau for testing **12** in the LORA assay, Hongye Li – for cloning GlcB into PDT vector, TAMU chemistry group currently lead by N. Zhou – for synthesizing ~ 400 compounds for this project, Tracey Musa – for comments on the manuscript, and the GSK team: Ortega, F. – for conducting PK experiments, Santos-Villarejo, A. – for plasma protein binding and stability experiments, Trullas, J. – for *in vivo* efficacy experiments, Alvarez-Gomez D. - for wild type enzyme testing, and Perez-Herranz, E. – for whole-cell H37Rv testing.

This work was funded by grants to Sacchettini, J.C.: by the Welch foundation, grant A-0015, by the NIH grant P01 AIO 68135, and by Global Alliance for TB Drug Development. Data were collected at Argonne National Laboratory, beamlines 19ID and 23ID.

References

- Adams PD, Grosse-Kunstleve RW, Hung LW, Ioerger TR, McCoy AJ, Moriarty NW, Read RJ, Sacchettini JC, Sauter NK, Terwilliger TC. PHENIX: building new software for automated crystallographic structure determination. *Acta Crystallogr D Biol Crystallogr*. 2002; 58:1948–1954. [PubMed: 12393927]
- Anstrom DM, Kallio K, Remington SJ. Structure of the Escherichia coli malate synthase G:pyruvate:acetyl-coenzyme A abortive ternary complex at 1.95 Å resolution. *Protein Sci*. 2003; 12:1822–1832. [PubMed: 12930982]
- Anstrom DM, Remington SJ. The product complex of M. tuberculosis malate synthase revisited. *Protein Sci*. 2006; 15:2002–2007. [PubMed: 16877713]
- Berryman OB, Bryantsev VS, Stay DP, Johnson DW, Hay BP. Structural criteria for the design of anion receptors: the interaction of halides with electron-deficient arenes. *J Am Chem Soc*. 2007; 129:48–58. [PubMed: 17199282]
- Beste DJV, Bonde B, Hawkins N, Ward JL, Beale MH, Noack S, Nöh K, Kruger NJ, Ratcliffe RG, McFadden J. C Metabolic Flux Analysis Identifies an Unusual Route for Pyruvate Dissimilation in Mycobacteria which Requires Isocitrate Lyase and Carbon Dioxide Fixation. *PLoS Pathog*. 2011; 7:e1002091. [PubMed: 21814509]
- Bloch H, Segal W. Biochemical differentiation of Mycobacterium tuberculosis grown in vivo and in vitro. *J Bacteriol*. 1956; 72:132–141. [PubMed: 13366889]
- Boudinot FD, Jusko WJ. Fluid shifts and other factors affecting plasma protein binding of prednisolone by equilibrium dialysis. *J Pharm Sci*. 1984; 73:774–780. [PubMed: 6204037]
- Bricogne, G, BE. BUSTER. version 2.9.2010.
- Carvalho, L.P.S. de; Fischer, SM.; Marrero, J.; Nathan, C.; Ehrt, S.; Rhee, KY. Metabolomics of Mycobacterium tuberculosis reveals compartmentalized co-catabolism of carbon substrates. *Chem Biol*. 2010; 17:1122–1131. [PubMed: 21035735]
- Cho SH, Warit S, Wan B, Hwang CH, Pauli GF, Franzblau SG. Low-oxygen-recovery assay for high-throughput screening of compounds against nonreplicating Mycobacterium tuberculosis. *Antimicrob Agents Chemother*. 2007; 51:1380–1385. [PubMed: 17210775]
- Clarke SE, Jeffrey P. Utility of metabolic stability screening: comparison of in vitro and in vivo clearance. *Xenobiotica*. 2001; 31:591–598. [PubMed: 11569527]
- Clark JD, O'Keefe SJ, Knowles JR. Malate synthase: proof of a stepwise Claisen condensation using the double-isotope fractionation test. *Biochemistry*. 1988; 27:5961–5971. [PubMed: 2847778]
- Copeland RA. Evaluation of enzyme inhibitors in drug discovery. A guide for medicinal chemists and pharmacologists. *Methods Biochem Anal*. 2005; 46:1–265. [PubMed: 16350889]
- Cox H, Ford N, Keshavjee S, et al. Rational use of moxifloxacin for tuberculosis treatment. *Lancet Infect Dis*. 2011; 11:259–260. [PubMed: 21453864]
- Dunn MF, Ramírez-Trujillo JA, Hernández-Lucas I. Major roles of isocitrate lyase and malate synthase in bacterial and fungal pathogenesis. *Microbiology*. 2009; 155:3166–3175. [PubMed: 19684068]
- Egbertson MS. HIV integrase inhibitors: from diketoacids to heterocyclic templates: a history of HIV integrase medicinal chemistry at Merck West Point and Merck Rome (IRBM). *Curr Top Med Chem*. 2007; 7:1251–1272. [PubMed: 17627556]
- Emsley P, Lohkamp B, Scott WG, Cowtan K. Features and development of Coot. *Acta Crystallogr D Biol Crystallogr*. 2010; 66:486–501. [PubMed: 20383002]
- Fischer E, Sauer U. A novel metabolic cycle catalyzes glucose oxidation and anaplerosis in hungry Escherichia coli. *Journal of Biological Chemistry*. 2001; 278(47):46446–51. [PubMed: 12963713]
- Franzblau SG, Witzig RS, McLaughlin JC, Torres P, Madico G, Hernandez A, Degnan MT, Cook MB, Quenzer VK, Ferguson RM, et al. Rapid, low-technology MIC determination with clinical Mycobacterium tuberculosis isolates by using the microplate Alamar Blue assay. *J Clin Microbiol*. 1998; 36:362–366. [PubMed: 9466742]
- Gengenbacher M, Rao SPS, Pethe K, Dick T. Nutrient-starved, non-replicating Mycobacterium tuberculosis requires respiration, ATP synthase and isocitrate lyase for maintenance of ATP homeostasis and viability. *Microbiology*. 2010; 156:81–87. [PubMed: 19797356]

- Gould TA, Langemheen H, van de, Muñoz-Elías EJ, McKinney JD, Sacchettini JC. Dual role of isocitrate lyase 1 in the glyoxylate and methylcitrate cycles in *Mycobacterium tuberculosis*. *Mol Microbiol*. 2006; 61:940–947. [PubMed: 16879647]
- Griffin JE, Gawronski JD, Dejesus MA, Ioerger TR, Akerley BJ, Sasseti CM. High-resolution phenotypic profiling defines genes essential for mycobacterial growth and cholesterol catabolism. *PLoS Pathog*. 2011; 7:e1002251. [PubMed: 21980284]
- Jackson MR, Beahm R, Duvvuru S, Narasimhan C, Wu J, Wang H-N, Philip VM, Hinde RJ, Howell EE. A preference for edgewise interactions between aromatic rings and carboxylate anions: the biological relevance of anion-quadrupole interactions. *J Phys Chem B*. 2007; 111:8242–8249. [PubMed: 17580852]
- Kornberg HL, Krebs HA. Synthesis of cell constituents from C2-units by a modified tricarboxylic acid cycle. *Nature*. 1957; 179:988–991. [PubMed: 13430766]
- Laskowski RA, Swindells MB. LigPlot+: Multiple ligand-protein interaction diagrams for drug discovery. *J. Chem. Inf. Model*. 2011; 51:2778–2786. [PubMed: 21919503]
- Marrero J, Rhee KY, Schnappinger D, Pethe K, Ehrst S. Gluconeogenic carbon flow of tricarboxylic acid cycle intermediates is critical for *Mycobacterium tuberculosis* to establish and maintain infection. *Proc Natl Acad Sci U S A*. 2010; 107:9819–9824. [PubMed: 20439709]
- McKinney JD, Bentrup K.H. zu, Muñoz-Elías EJ, Miczak A, Chen B, Chan WT, Swenson D, Sacchettini JC, Jacobs WR, Russell DG. Persistence of *Mycobacterium tuberculosis* in macrophages and mice requires the glyoxylate shunt enzyme isocitrate lyase. *Nature*. 2000; 406:735–738. [PubMed: 10963599]
- Motyl M, Dorso K, Barrett J, Giacobbe R. Basic Microbiological Techniques Used in Antibacterial Drug Discovery. *Current Protocols in Pharmacology*. 2006
- Muñoz-Elías EJ, McKinney JD. *Mycobacterium tuberculosis* isocitrate lyases 1 and 2 are jointly required for in vivo growth and virulence. *Nat Med*. 2005; 11:638–644. [PubMed: 15895072]
- Murshudov GN, Skubák P, Lebedev AA, Pannu NS, Steiner RA, Nicholls RA, Winn MD, Long F, Vagin AA. REFMAC5 for the refinement of macromolecular crystal structures. *Acta Crystallogr D Biol Crystallogr*. 2011; 67:355–367. [PubMed: 21460454]
- Núñez MF, Pellicer MT, Badia J, Aguilar J, Baldoma L. Biochemical characterization of the 2-ketoacid reductases encoded by *ycdW* and *yiaE* genes in *Escherichia coli*. *Biochem J*. 2001; 354:707–715. [PubMed: 11237876]
- Obach RS, Baxter JG, Liston TE, Silber BM, Jones BC, MacIntyre F, Rance DJ, Wastall P. The prediction of human pharmacokinetic parameters from preclinical and in vitro metabolism data. *J Pharmacol Exp Ther*. 1997; 283:46–58. [PubMed: 9336307]
- Otwinowski Z, Minor W. Processing of X-ray Diffraction Data Collected in Oscillation Mode. *Methods in Enzymology*. 1997; 276:307–326.
- Payne DJ, Gwynn MN, Holmes DJ, Pompliano DL. Drugs for bad bugs: confronting the challenges of antibacterial discovery. *Nat Rev Drug Discov*. 2007; 6:29–40. [PubMed: 17159923]
- Pettersen EF, Goddard TD, Huang CC, Couch GS, Greenblatt DM, Meng EC, Ferrin TE. UCSF Chimera—a visualization system for exploratory research and analysis. *J Comput Chem*. 2004; 25:1605–1612. [PubMed: 15264254]
- Philip V, Harris J, Adams R, Nguyen D, Spiers J, Baudry J, Howell EE, Hinde RJ. A survey of aspartate-phenylalanine and glutamate-phenylalanine interactions in the protein data bank: searching for anion- π pairs. *Biochemistry*. 2011; 50:2939–2950. [PubMed: 21366334]
- Quartararo CE, Blanchard JS. Kinetic and chemical mechanism of malate synthase from *Mycobacterium tuberculosis*. *Biochemistry*. 2011; 50:6879–6887. [PubMed: 21728344]
- Rullas J, García JI, Beltrán M, Cardona PJ, Cáceres N, García-Bustos JF, Angulo-Barturen I. Fast standardized therapeutic-efficacy assay for drug discovery against tuberculosis. *Antimicrob Agents Chemother*. May; 2010 54(5):2262–4. 2010. [PubMed: 20160054]
- Sacchettini JC, Rubin EJ, Freundlich JS. Drugs versus bugs: in pursuit of the persistent predator *Mycobacterium tuberculosis*. *Nat Rev Microbiol*. 2008; 6:41–52. [PubMed: 18079742]
- Sakuraba H, Yoneda K, Takeuchi K, Tsuge H, Katunuma N, Ohshima T. Structure of an archaeal alanine:glyoxylate aminotransferase. *Acta Crystallogr D Biol Crystallogr*. 2008; 64:696–699. [PubMed: 18560158]

- Sambandamurthy VK, Derrick SC, Hsu T, Chen B, Larsen MH, Jalapathy KV, Chen M, Kim J, Porcelli SA, Chan J, et al. Mycobacterium tuberculosis DeltaRD1 DeltapanCD: a safe and limited replicating mutant strain that protects immunocompetent and immunocompromised mice against experimental tuberculosis. *Vaccine*. 2006; 24:6309–6320. [PubMed: 16860907]
- Schnappinger D, Ehrt S, Voskuil MI, Liu Y, Mangan JA, Monahan IM, Dolganov G, Efron B, Butcher PD, Nathan C, et al. Transcriptional Adaptation of Mycobacterium tuberculosis within Macrophages: Insights into the Phagosomal Environment. *J Exp Med*. 2003; 198:693–704. [PubMed: 12953091]
- Schottel BL, Chifotides HT, Dunbar KR. Anion-pi interactions. *Chem Soc Rev*. 2008; 37:68–83. [PubMed: 18197334]
- Sharma V, Sharma S, Bentrup K.H. zu, McKinney JD, Russell DG, Jacobs WR, Sacchettini JC. Structure of isocitrate lyase, a persistence factor of Mycobacterium tuberculosis. *Nat Struct Biol*. 2000; 7:663–668. [PubMed: 10932251]
- Smith CV, Huang C, Miczak A, Russell DG, Sacchettini JC, Bentrup K.H. zu. Biochemical and structural studies of malate synthase from Mycobacterium tuberculosis. *J Biol Chem*. 2003; 278:1735–1743. [PubMed: 12393860]
- Talaat AM, Lyons R, Howard ST, Johnston SA. The temporal expression profile of Mycobacterium tuberculosis infection in mice. *Proc Natl Acad Sci U S A*. 2004; 101:4602–4607. [PubMed: 15070764]
- Timm J, Post FA, Bekker L-G, Walther GB, Wainwright HC, Manganelli R, Chan W-T, Tsenova L, Gold B, Smith I, et al. Differential expression of iron-, carbon-, and oxygen-responsive mycobacterial genes in the lungs of chronically infected mice and tuberculosis patients. *Proc Natl Acad Sci U S A*. 2003; 100:14321–14326. [PubMed: 14623960]
- Wayne LG, Lin KY. Glyoxylate metabolism and adaptation of Mycobacterium tuberculosis to survival under anaerobic conditions. *Infect Immun*. 1982; 37:1042–1049. [PubMed: 6813266]
- Yazdanian M, Glynn SL, Wright JL, Hawi A. Correlating partitioning and caco-2 cell permeability of structurally diverse small molecular weight compounds. *Pharm Res*. 1998; 15:1490–1494. [PubMed: 9755906]
- World Health Organization. Global Tuberculosis Control 2011. Switzerland; Geneva: 2011. http://www.who.int/tb/publications/global_report/en/
- Zeng L-F, Jiang X-H, Sanchez T, Zhang H-S, Dayam R, Neamati N, Long Y-Q. Novel dimeric aryldiketo containing inhibitors of HIV-1 integrase: effects of the phenyl substituent and the linker orientation. *Bioorg Med Chem*. 2008; 16:7777–7787. [PubMed: 18644730]
- Collaborative Computational Project, Number 4. *Acta Cryst*. 1994; D50:760–763.

Highlights

- discovery and stabilization of phenyl diketo-acid (PDKA) inhibitors for GlcB
- exploring binding interactions and improving potency through structure-based design
- PDKAs are bactericidal to *Mtb* grown on fatty acids and carbohydrates
- targeting GlcB with PDKA reduces bacterial load in a mouse model of tuberculosis.

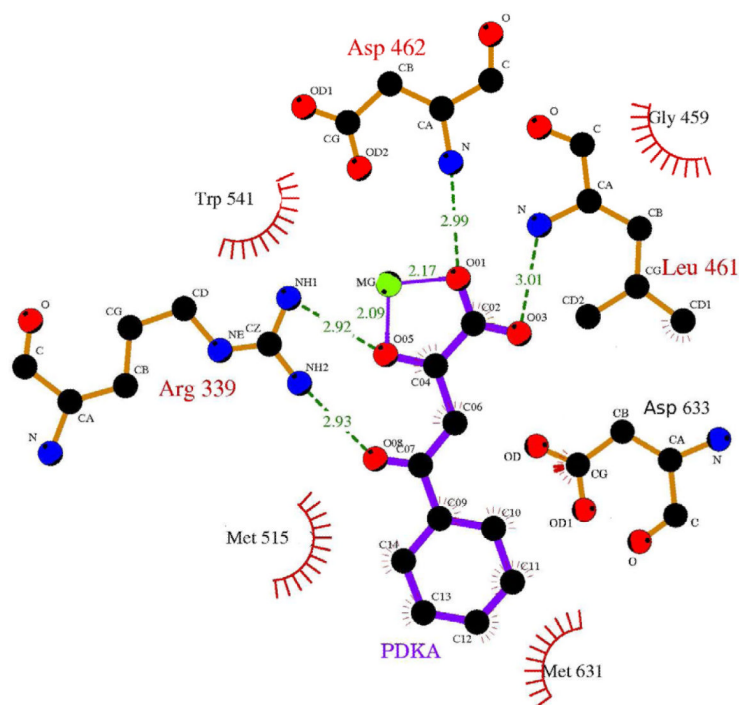
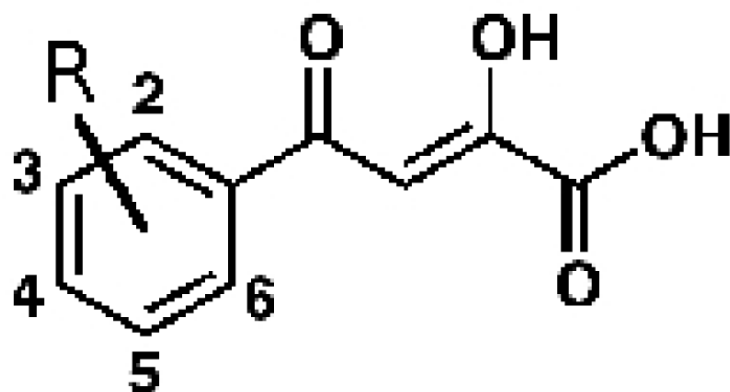


Figure 1. PDKA inhibitor and its contacts to GlcB

A - PDKA chemical structure drawn here in the enol form most consistent with solution-phase ^1H and ^{13}C NMR data; **B** – diagram of PDKA–GlcB interactions; hydrogen bonds are shown in green. Catalytic Asp633 contacts the face of the phenyl ring. Coordinating interactions between the Mg^{2+} ion and oxygens of the inhibitor are in purple. Atom colors: black=carbon, red=oxygen, blue=nitrogen, green=magnesium. This figure was made in LigPlot (Laskowski and Swindells, 2011).

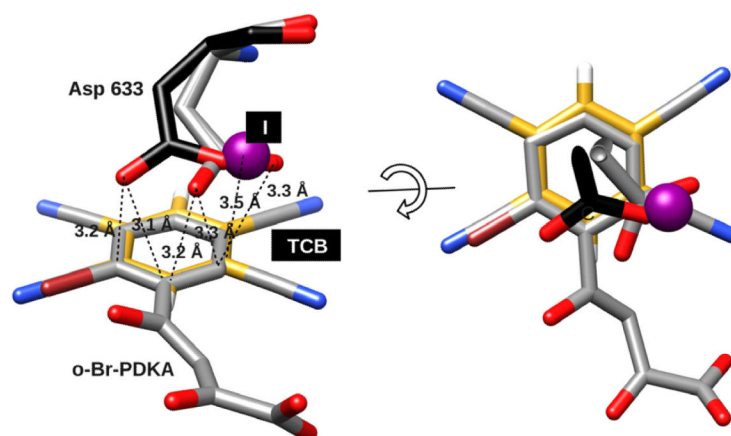


Figure 2. Anion- π interaction

PDKA inhibitor (4) with Asp633 superimposed with crystal structure of tetracyanobenzene (TCB) in complex with NaI (606750 entry at Cambridge Crystallographic Data Center as supplementary for small molecule anion- π complex structures (Berryman et al., 2007)) colored by element, TCB ring is slightly off-set for easier visualization. Halide shown as a purple sphere, TCB carbons are colored yellow; Asp633 with gray carbons represent Asp633 position in complex with single ortho-halogen substituted PDKAs (o-Br-PDKA shown), while Asp633 with black carbons represent Asp633 position for all other complexes (with PDKA, 1, 7 and 11). Atom colors: black, gray or yellow=carbon, red=oxygen, blue=nitrogen, white=hydrogen, purple=iodine. Images rendered in CHIMERA (Pettersen et al., 2004).

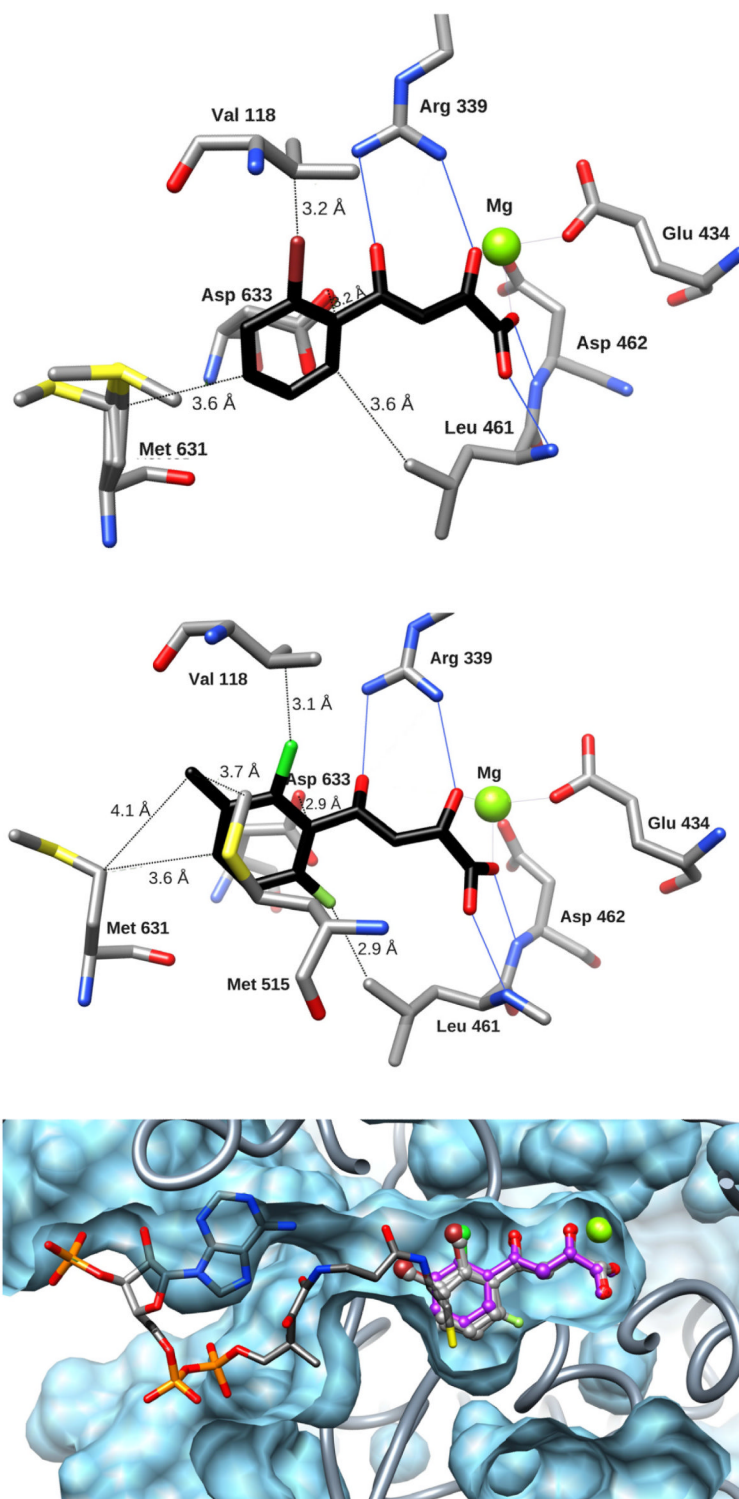


Figure 3. Comparing binding of PDKA analogs to GlcB

Binding of GlcB to inhibitor **4** (A) and inhibitor **11** (B) colored by element, with C_{protein} in grey, and C_{ligand} in black. Hydrogen bonds are indicated by solid blue lines, distances from key positions on the phenyl ring to protein residues are marked as dashed lines. (C) - Crystal

structure overlay of GlcB complexed with PDKA (in magenta), **1**, **4**, **7**, **11** – represented in ball-and-stick, and CoA represented by a stick model (colored by element), with the Mg atom in green, illustrate the relative positions of the ligands occupying the active site channel (presented by protein surface calculated in CHIMERA (Pettersen et al., 2004)). The CoA model and protein surface were made from chain A of the 2GQ3 model.

Table 1

Stability and activity data for PDKA family inhibitors.

Compound	R	Half-life (days)	λ_{\max} (nM)	IC ₅₀ (nM)	MIC ₉₉ mc ² -7000 <i>Mtb</i> acetate (μ M)	MIC ₉₉ mc ² -7000 <i>Mtb</i> dextrose (μ M)
PDKA	Ph	3	340	2.0	50	25
1	2-MePh	30	326	1.1	>200	200
2	2-FPh	12	333	0.24	>200	200
3	2-ClPh	35	324	0.5	>200	200
4	2-BrPh	18	324	0.6	6.25	12.5
5	3-MePh	11	339	0.18	25	50
6	3-ClPh	7	341	0.17	25	25
7	3-BrPh	7	341	0.8	25	25
8	4-MePh	8	340	6.0	50	100
9	4-BrPh	7	345	5.7	50	25
10	2-Cl-6-FPh	>30	317	2.7	50	100
11	2-Cl-6-F-3MePh	>30	321	5.5	50	100

Table 2

Crystal data collection and refinement statistics

Data restricted to highest resolution shell are shown in parentheses. All crystals were of the C619A mutant enzyme with His₆ tag.

Data collection	GlcB complex with PDKA	GlcB complex with 4	GlcB complex with 1	GlcB complex with 7	GlcB complex with 11
Space group	P4 ₃ 2 ₁ 2	P4 ₃ 2 ₁ 2	P4 ₃ 2 ₁ 2	P4 ₃ 2 ₁ 2	P4 ₃ 2 ₁ 2
Cell dimensions					
<i>a</i> , <i>b</i> , <i>c</i> (Å)	79.33, 79.33, 225.94	79.45, 79.45, 226.26	77.74, 77.74, 221.98	78.22, 78.22, 223.58	78.49, 78.49, 224.05
<i>a</i> , <i>b</i> , <i>g</i> (°)	90, 90, 90	90, 90, 90	90, 90, 90	90, 90, 90	90, 90, 90
Resolution (Å)	50-1.90 (1.93-1.9)	43.05-1.80 (1.83-1.80)	44.13-1.82 (1.92-1.82)	49.57-2.04 (2.13-2.04)	45.59-2.20 (2.24-2.20)
<i>R</i> _{sym} or <i>R</i> _{merge}	0.109 (0.532)	0.191 (0.634)	0.108 (0.554)	0.099 (0.584)	0.183 (0.742)
<i>I</i> / <i>σ</i>	13.8	14.0	6.4	6.3	9.0
Completeness (%)	99.9 (99.4)	97.2 (76.0)	99.9 (100)	99.2 (98.6)	99.9 (100)
Redundancy	13.1 (10.2)	9.5 (2.6)	9.7 (9.8)	15.3 (15.4)	14.4 (14.8)
Refinement					
Resolution (Å)	50-1.90	43.05-1.8	44.13-1.82	49.57-2.04	45.59-2.2
No. reflections	57789	66563	62029	45023	36507
<i>R</i> _{work} / <i>R</i> _{free}	0.1678/0.2027	0.1753/0.2192	0.1704/0.2196	0.1628/0.2040	0.1721/0.2231
No. atoms					
Protein	5543	5645	5562	5509	5429
Ligand/ion	14/3	15/3	15/3	15/3	17/3
Water	674	859	641	574	400
B-factors					
Protein	27.86	29.64	21.22	32.13	34.69
Ligand/ion	30.47/28.14	20.7/32.13	14.24/27.53	30.1/38.4	28.87/39.3
Water	39.65	40.55	28.79	38.58	40.78
R.m.s deviations					
Bond lengths (Å)	0.013	0.007	0.007	0.007	0.008
Bond angles (°)	1.03	1.024	1.013	1.013	1.062

Table 3

H37Rv activity, mouse plasma protein binding, and mouse microsomes clearance data for alkyl- and benzyl-ester prodrugs of selected PDKA analogs.

compound	H37Rv MIC ₉₉ on acetate (μM)	H37Rv MIC ₉₉ on dextrose (μM)	Mouse microsomes clearance (ml/min*gr)	Mouse plasma protein binding (%)
11	16	31	< 0.3	70 ± 3.0
Me ester of 11 (12)	2	8	0.6 ± 0.2	91.9 ± 1.6
Benzyl ester of 11	< 1	2	> 30	ND
4	16	31	< 0.3	67.5 ± 2.6
Me ester of 4	8	16	3.2 ± 0.7	87.7 ± 1.6
Benzyl ester of 4	<1	8	15.3 ± 6.1	ND
1	16	31	ND	70.7 ± 1.8
Me ester of 1	4	16	4.6 ± 0.7	87.1 ± 1.4
Benzyl ester of 1	<1	16	>30	ND

Table 4

Therapeutic efficacy of 12 against Mtb in mice

Five animals in each testing group were inoculated with 10^5 colony-forming units (CFU) of *Mtb* intratracheally, and treatment started one day post-infection. Nine days post-infection the mice were sacrificed and the respective bacterial loads in the lungs were determined. All reductions in CFU were statistically significant over the untreated control group by a T-test (dof=9-10, '**' indicates $p < 0.0001$).

Compound	Target dose (mg/kg)	Experimental dose (mg/kg)	Administration	Decrease in log ₁₀ CFU in lungs	Standard error
Moxifloxacin	30	36	Once a day	3.07*	0.0639
12	500	542	Once a day	1.68*	0.103
12	600	718	Once a day	1.72*	0.149
12	300	377	Twice a day	1.89*	0.0787
12	400	460	Twice a day	2.12*	0.108